SSIM 2023 – PM Dight (ed.)

doi:10.36487/ACG_repo/2335_50

Observing the anatomy of slope failure using time-lapse seismic velocity changes

G Taylor *Institute of Mine Seismology, Australia*

T de Wit *Institute of Mine Seismology, Australia*

Abstract

The seismic velocity of an Earth material is a key physical characteristic that can provide critical information such as composition, porosity, and overall cohesion of said material. Although such physical properties are typically assumed to be static in time for any given rock mass, it has been observed that the seismic velocity of natural materials can vary with time in response to a variety of processes, which can include environmental, anthropogenic, or tectonic effects. Such processes may include stress-induced slip events or changes in pore fluid pressure. The temporal changes in seismic velocity that result from these effects are typically extremely small (<1%), and are therefore difficult to observe reliably. The best approach to observing temporal seismic velocity variations within a medium does not involve the measurement of travel time delays in direct waves from ballistic seismic events, but instead focuses on multiple scattered waves contained within the ambient seismic noise field. We present a novel experiment in which continuous recordings of ambient seismic noise made within the open pit wall of the Century Mine in Australia are used to track variations in seismic velocity during a period of substantial failure in the stability of the pit wall. We observe a decrease in the bulk seismic velocity of 0.5% during the course of the failure, with the onset of this decrease occurring approximately two weeks prior to the initiation of major surface deformation. The precursory decrease in seismic velocity begins following a nearby mining blast and precedes the onset of other geophysical signals that herald the slope failure, including conventional seismic monitoring, and geodetic observations. We propose that the routine monitoring of seismic velocity variations may be provide critical information, including early warning, in the management of landslide hazards.

Keywords: *slope monitoring and its interpretation, slope stability in weak rocks and rock dumps, case studies*

1 Introduction

Landslides are widespread geological events that directly impact thousands of people every year and cause significant loss of life. Landslides have frequently been recorded as externally triggered by such events as extreme weather and earthquakes. Surface mining environments often contain steep open pit walls located in close proximity to operations that may induce seismic ground motions, either through blasting or natural seismic events. As surface mines are also typically open to the elements, they are by their very nature particularly vulnerable to landslide-related hazards. The increased hazard of landslides in surface mining environments necessitates a strong understanding of the internal kinematics of rock masses that may be at risk of failure, so that landslide hazard may be mitigated appropriately.

Most modern slope monitoring techniques are geodetic in nature, focusing on deformation at the surface of the landslide. Though geodesy can provide critical information on the rheology of a landslide, and give early warning prior to a dangerous failure, there is the possibility that by the time changes manifest at surface, it can be too late to effectively mitigate the growing hazard. Geodetic measurements also provide no constraint on the internal geological structure that may have a drastic impact on the development of a landslide.

Passive seismic ambient noise techniques have been successfully applied in landslide monitoring (Le Breton et al. 2021). Ambient noise methods can be used to measure time-lapse changes in seismic velocity within

the subsurface of a slope. These seismic velocity variations are directly sensitive to the fluctuating mechanical properties of the rock mass. As a result of this sensitivity, it is possible to detect precursory changes in the medium that may be utilised to provide early warning of failure.

We present a case study from a dense borehole geophone array installed beneath the well-instrumented slope of the Century open pit mine in north-west Queensland, Australia. We apply the seismic ambient-noise method to extract time-lapse seismic velocity variations throughout a period of slope failure. We then combine our observations of temporal variations in seismic velocity with a simple model of seismic scattering to estimate the spatial distribution of changing mechanical properties throughout the pit wall. Our results are interpreted to present a proof-of-concept of the ability to use observations of seismic velocity variations as an early warning system for slope instability for mining environments. By mapping the spatial distribution of these variations, we also demonstrate the importance of pre-existing geological structures that can localise deformations during failure and provide significant control upon the dynamics of slope stability.

2 Methodology

2.1 Spatially averaged seismic velocity variations

In this study, we used continuous seismic data recorded at an array of 16 geophones that were installed in boreholes drilled into the western perimeter of the open pit wall at Century Mine (Figure 1). The intended purpose of the seismic array was to undertake routine monitoring of microseismic events that may occur in the rock mass behind the pit wall (Luo et al. 2018; Salvoni & Dight 2016). Here we utilised the continuous seismic data that was recorded at a sampling rate of 6,000 Hz to perform seismic interferometry and derive estimates of the temporal variability in the seismic velocity of the pit wall.

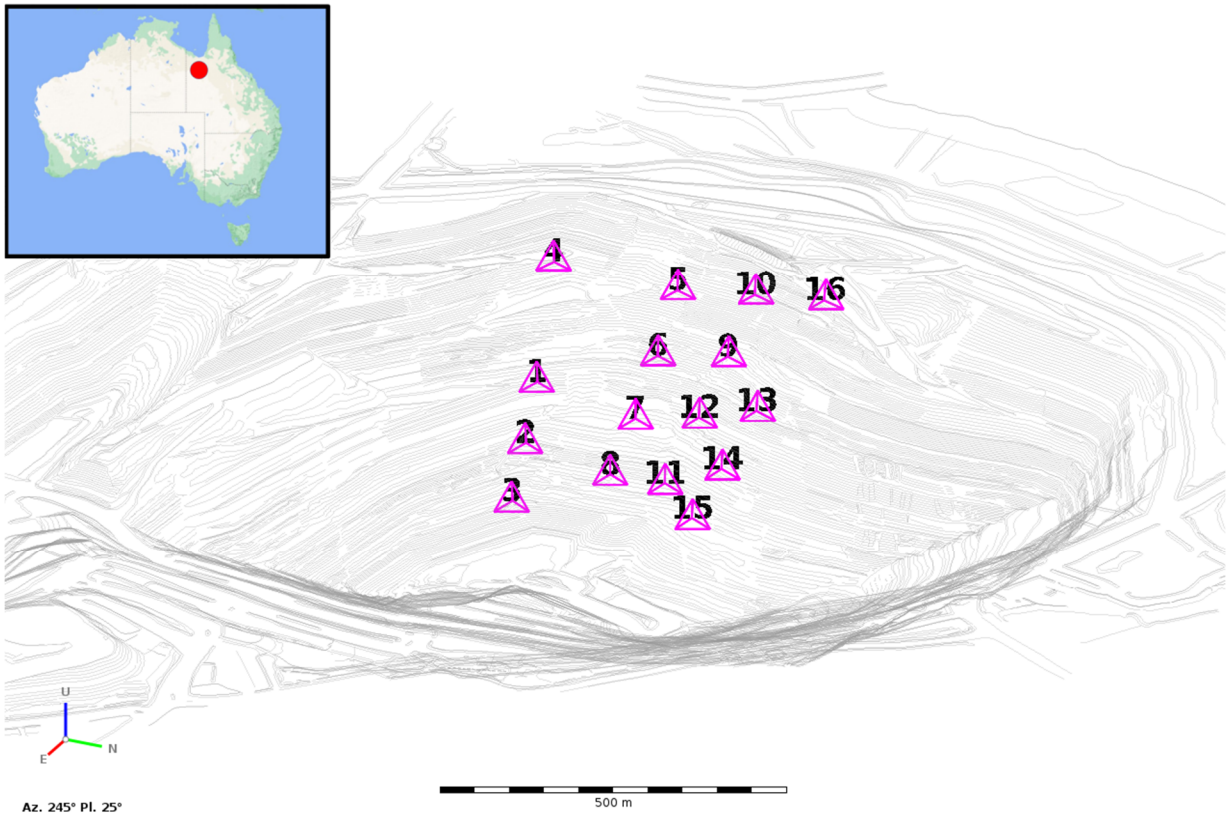

Figure 1 Locations of borehole geophones installed within the western pit wall of Century Mine. The view is towards the north-west

To process the continuous data, we first down-sample the ground velocity recordings to 500 Hz, and cut them into 10-second long windows. We remove the mean and the linear trend of each 10-second window. We then follow the established practice of generating cross-correlation functions from ambient seismic noise data as outlined in detail by Bensen et al. (2007). The amplitudes of the records are 'one-bit' normalised, that is, the absolute amplitude is discarded and only the sign of the ground motion is retained. The frequency spectra of the ground motion windows are also whitened in the frequency band 5–100 Hz to balance the contributions of different noise sources. Each 10-second long window at a given sensor is then cross-correlated with the corresponding time window at every other sensor in the array to provide a cross-correlation function for that time period. We then average the suite of cross-correlation functions in non-overlapping two-day periods. Overall, this process yields an observed cross-correlation function between each sensor pair for every two-day time window throughout the analysis period. An example of the waveforms of these cross-correlation functions between Sensor 1 and Sensor 3 is shown in Figure 2.

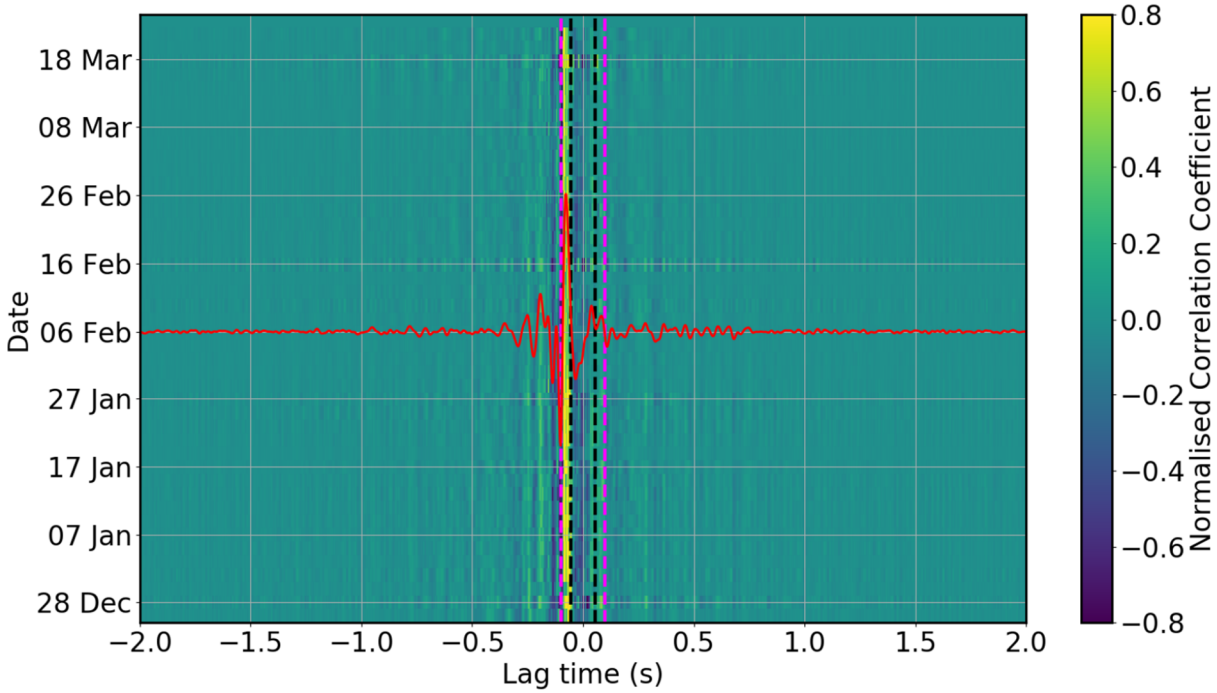

Figure 2 Cross-correlation waveforms between Sensor 1 and Sensor 3 for correlation lags between −2 s and 2 s between 25 December 2013 and 31 March 2014. The red waveform shows the average cross-correlation function for this time period. The black dashed line indicates the estimated arrival time for a direct P-wave travelling at 3.6 km/s. The red dashed line is the arrival time for an S-wave with a velocity of 2.0 km/s

To measure temporal variations in seismic velocity from the resulting cross-correlation functions, we apply the moving window cross-spectrum (MWCS) method (Clarke et al. 2011). The MWCS approach measures the time delay (δt) that affects the multiple scattered waves present in two separate cross-correlation functions. To generate robust time-delay measurements, we apply the MWCS method to the multiple scattered waves that arrive at late lag times in the cross-correlation functions immediately following the direct S-wave arrival (Figure 2). We measure delay times on both the positive and negative correlation lags up to a maximum lag time of 2 s. The measurement window is 0.17 s long, which is run along the cross-correlation function with a window overlap of 0.02 s (90%) to increase the number of time-delay observations and reduce the uncertainty of the estimate. The time-delay measurement in each MWCS window contributes a data point to the full suite of measurements taken on a given cross-correlation function, upon which we can perform a weighted linear regression to obtain an estimate of the relative time delay $\delta t/t$ between two cross-correlation functions (in our case, every two days). Clarke et al. (2011) show that if these time delays are assumed to be the result of a homogeneous variation in seismic velocity

within the medium, then the relative change in seismic velocity can be simply related to the relative time delay by $\delta v/v = -\delta t/t$.

As we are dealing with relative variations in seismic velocity, we must define some reference state that the time shifts in our individual cross-correlation functions can be compared with. In this case, we construct a reference waveform by averaging all of the two-day cross-correlation functions for the entire analysis period (Figure 2). Figure 2 shows the resulting relative seismic velocity change measurements between Sensor 1 and Sensor 3 for the period spanning 25 December 2013 to 31 March 2014.

2.2 Localisation of seismic velocity variations in space

The approach outlined in Section 2.1 is sufficient for describing the temporal variability of seismic velocity as averaged throughout the entire rock mass. While useful, this average measurement reveals little about the spatial distribution of these seismic velocity variations. This spatial distribution of temporal variations in material properties is of critical importance in understanding the physics of landslides, which are often believed to initiate along pre-existing weak geological structures. The ability to understand the progression of a landslide in four dimensions represents a key component of managing landslide risk.

It is possible to derive a relationship between the observed time delays of scattered waves travelling between two seismic sensors (as described in Section 2.1) and the location of the perturbation in the rock medium that caused said time delay. By making multiple time-delay measurements from several seismic sensors, we can combine this information to map the spatial changes in the seismic velocity of a three-dimensional rock mass. Pacheco & Snieder (2005) showed that the suite of time-delay observations can be related to the 3D distribution of seismic velocity changes by:

$$\frac{\delta t}{t} = \frac{\delta V}{t}\frac{\delta v}{v}K \tag{1}$$

where $\delta t/t$ are our measured relative time delays, t is the arrival time of the wave for which $\delta t/t$ is measured, δV is the volume of our expected rock mass perturbations and δv/v is the target 3D distribution of seismic velocity variations. The key relationship between $\delta t/t$ and $\delta v/v$ is the sensitivity kernel K, which is defined by:

$$K(S,R,r_0,t) = \frac{\int_0^t P(S,r_0,t)P(r_0,R,t)}{P(S,R,t)} \tag{2}$$

where the functions *P(a, b, t)* represent the scattering intensity between point a and point b as a function of time. The relevant points in space are the source location S, the receiver location R and the location of the velocity perturbation r_0.

If we assume that the scattered energy propagates under a simple physical scheme, such as the diffusion or radiative transfer approximations, analytical formulae exist for these scattering intensities. For example, under the diffusion approximation, the scattering intensities required to calculate the sensitivity kernel K in Equation 2 would be given by:

$$P(r,t) = \frac{1}{4\pi D t^{3/2}} exp\left(\frac{-r^2}{Dt}\right) \tag{3}$$

where D is the diffusion constant of the medium, and r is the distance between the two points under consideration. In the following analysis, we use the slightly more complex physical system known as radiative transfer. The radiative transfer approximation is a modification to the diffusion approximation in Equation 3 and is preferred because it more accurately models the sharp, high amplitude onset that marks the initial arrival of scattered energy in a seismogram. The full analytical formula for scattering intensity under radiative transfer is given in Equation 36 of Paasschens (1997). Strictly, the diffusion and radiative transfer approximations define scattering intensities in an infinite medium. To properly account for the presence of a free surface in an open pit mining environment, the infinite solution is calculated, and the scattering intensity calculated for regions above the free surface are reflected about the free surface and summed to the intensities already within the medium (Obermann et al. 2013).

Following the correct calculation of the sensitivity kernel *K*, the system of linear equations described by Equation 1 can be solved for the desired spatial distribution of seismic velocity changes, *δv/v.* Any appropriate inverse method can be used to calculate the best-fitting distribution of *δv/v*. In our approach, we opted to solve the system using an inversion scheme based on singular value decomposition. The singular value decomposition approach is suitable in this case because we are typically trying to invert for a number of model parameters (velocity variations in a 3D medium) that far exceeds our number of independent observations (time delays between a given set of seismic sensors). Using these results, we have developed a workflow to invert a set of relative time-delay measurements made at several sensor locations for the corresponding best-fitting 3D estimate of seismic velocity changes between two points in time.

3 Results

3.1 Time-lapse variations in seismic velocity in the open pit wall

Figure 3a shows a time series of relative seismic velocity variations within the Century Mine pit wall between 25 December 2013 and 31 March 2014. The velocity variations shown in Figure 3a are produced by averaging the individual time series across all sensor pairs. The general character of the seismic velocity variations within the pit wall is that of small (<0.05%) stable velocity variations between December 2013 and 9 February 2014. Following the two-day period of 9 February to 11 February 2014, a steady decrease in relative seismic velocity was observed. This decreasing trend in seismic velocity was sustained for the remainder of the analysis period until 31 March 2014. Between 9 February and 31 March 2014, seismic velocity in the pit wall decreased by approximately 0.5%. The onset of the seismic velocity decrease occurs within the same two-day period as a mining blast performed at the foot of the pit wall on 11 February 2014. The timing of this blast is also indicated in Figure 3.

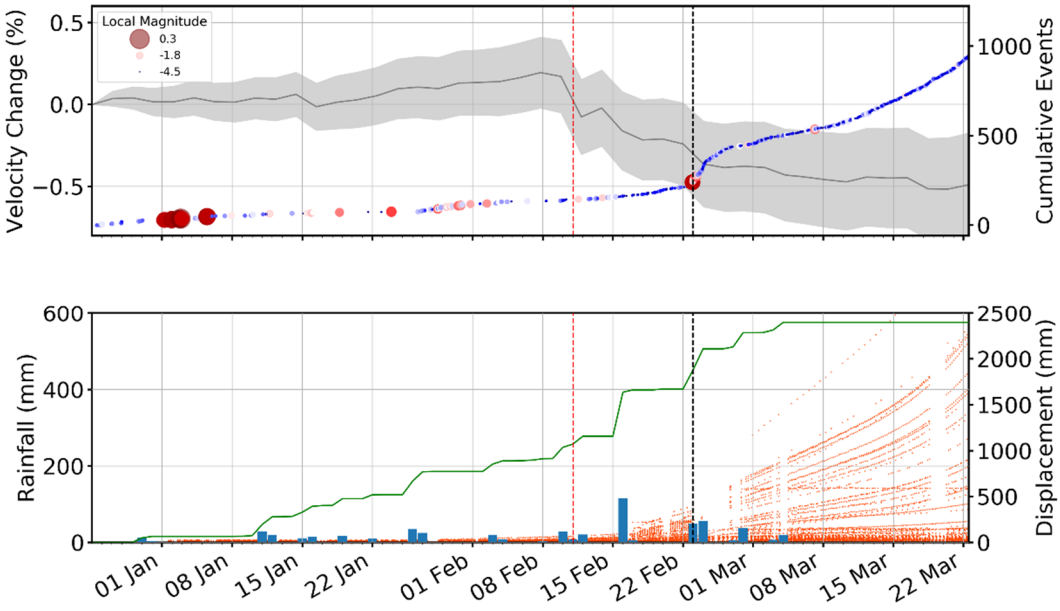

Figure 3 (a) Time-lapse seismic velocity changes averaged across all sensor pairs between 25 December 2013 and 31 March 2014 (grey line). The grey shaded region indicates the cumulative uncertainty in the measurements. Also shown is the cumulative number of seismic events that occurred at Century Mine during the analysis period, coloured and sized by the local magnitude. (b) Total daily rainfall (blue bars) and cumulative daily rainfall (green) measured at Century Mine by the Australian Bureau of Meteorology station designated YCNY (Century Mine). Orange dots are the line-of-sight surface displacement of the pit wall measured by ground-based radar (Salvoni & Dight 2013). Red dashed lines indicates the timing of a mining blast at the foot of the pit wall. The black dashed line is the interpreted start time of slope failure

3.2 Time-lapse variations in seismic velocity in the open pit wall

Figure 4 shows the estimated distribution of relative seismic velocity variations between 25 December 2013 and 2 March 2014 (10 days after the slope was interpreted as failing, based on ground radar measurements). Figure 4 displays the seismic velocity variations projected over the topography of the open pit wall. Also shown in Figure 4 are the surface expressions of two major fault structures within the pit wall: the Page Creek Fault and the Pandora Fault. It is clear from Figure 4 that long-term distributed seismic velocity changes resulting from the slope failure are in the order of 0.01%. It is also clear that the seismic velocity variations are not uniformly distributed throughout the rock mass of the pit wall. The largest reductions in seismic velocity occurred in the vicinity of the Pandora Fault, about halfway up the pit wall face, within a distinct unit of breccia. In contrast, seismic velocity can be seen to have increased near the rim of the pit wall and in the buttress located at the foot of the wall. It is also clear that both the Page Creek Fault and the Pandora Fault delineate sharp boundaries in the observed spatial pattern of seismic velocity changes. The material located within the zone between the two faults, apart from the carbonaceous breccia (CBX) block, generally experienced an increase in seismic velocity. Material located in the exterior of the two faults generally decreased in seismic velocity.

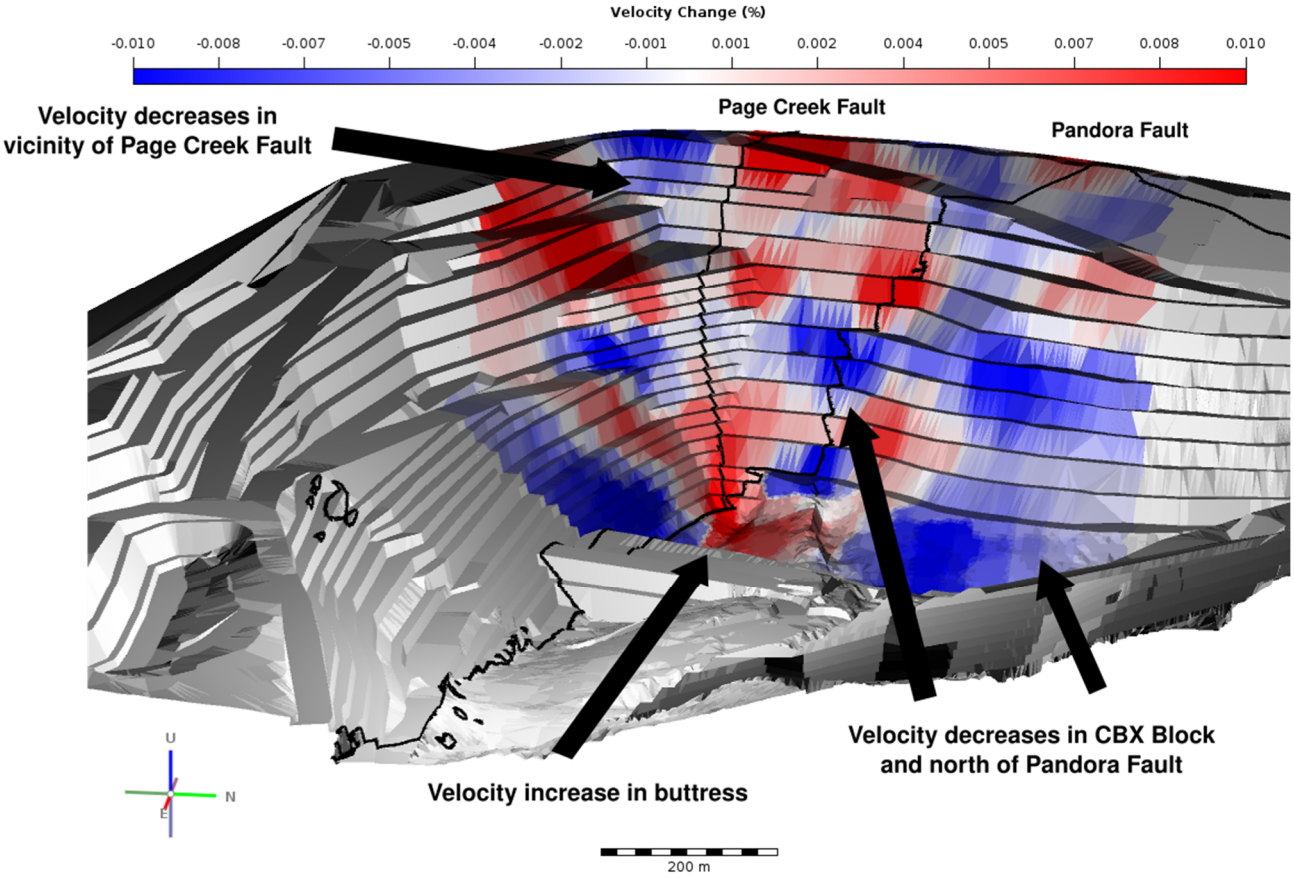

Figure 4 Spatial distribution of relative seismic velocity changes that occurred within the pit wall at Century Mine between 25 December 2013 and 2 March 2014 (10 days after slope failure). Blue colours indicate decreases in seismic velocity; red colours indicate increases. The thick black lines show the surface expression of the Page Creek and Pandora fault systems. Annotations indicate general features of the spatial variation in seismic velocity changes

4 Discussion

The spatially averaged time-lapse seismic velocity changes shown in Figure 3a exhibit a robust and sustained decrease after 9 to 11 February 2014. The onset of this decrease clearly precedes the detection of significant surface displacements along the pit wall, which were detected by ground-based radar and which began, at the earliest, on 16 February 2014. The bulk decrease in seismic velocity also occurred prior to the initiation of the second period of significant seismicity on 23 February, which was also accompanied by an acceleration in surface displacements and interpreted as marking the beginning of slope failure.

The seismic velocity decrease within the pit wall begins after a mine blast was carried out at the foot of the of the slope on 11 February 2014. Seismic velocity decreases associated with co-seismic damage of shallow geological layers incurred by ground shaking are a common observation in regional tectonic settings (Brenguier et al. 2008; Taylor & Hillers 2019). Although it is likely that there would be a decrease in seismic velocity within the pit wall, which occurs as a direct result of ground shaking associated with the blast, it is notable that the velocity decrease is sustained for a period of 12 days until the major slope failure occurred, and does not appear to return to a steady state until 31 March 2014. The sustained decrease in seismic velocity indicates further processes are likely to play a role, as velocity decreases associated with co-seismic damage typically exhibit a subsequent logarithmic increase in seismic velocity as the rock mass 'heals' (Snieder et al. 2017). Possible mechanisms for the persistent decrease in seismic velocity could include the continued infiltration of fluids into existing fault structures, or newly opened cracks, following rainfall events, which can be expected to induce pore pressure variations within the rock mass.

The hypothesis that the sustained decrease in seismic velocity could be related to variations in the physical properties of pre-existing geological structures is supported by the spatial distribution of long-term seismic velocity changes that occurred as a result of the slope failure shown in Figure 4. The distinct geological structures located within the pit wall at Century Mine appear to be exerting some form of control over the location of material property variations. The largest decreases in seismic velocity are associated with a large block of breccia situated halfway up the pit wall. This breccia block was referred to as the CBX block by Salvoni & Dight (2016), who observed the block to act as a wedge that controlled deep-seated failure within the pit wall. The seismic velocity reduction in the CBX block may be the result of rock fracturing as it is placed under stress during the slope failure. By contrast, the relative seismic velocity increase observed in the buttress at the foot of the pit wall may indicate some degree of fracture closure caused by an increase in compressive stress in the buttress.

The Page Creek and Pandora fault systems are generally associated with general decreases in seismic velocity following the slope failure, though also appear to mark sharp boundaries in the nature of the overall response. Between the two faults, and excepting the CBX breccia block, seismic velocity was observed to increase, particularly near the upper rim of the pit wall. Outside of the fault systems, two sub-vertical linear zones exhibit moderate decreases in seismic velocity (~0.05%). It is possible that the fault systems act as conduits to meteoric fluids introduced during rainfall events, that may subsequently penetrate the surrounding geological units if the state of stress in such that a permeable fracture system exists. Although the precise mechanisms driving the variation in seismic velocity across the pit wall following the slope failure remain difficult to interpret, it is clear that pre-existing geological structures likely play a key role in the distribution of stress throughout the rock mass.

5 Conclusion

This study has presented observations of time-lapse variations in seismic velocity within the open pit wall at Century Mine during a period of active slope failure. Such variations in seismic velocity provide critical information on the physical properties of the rocks and on how they respond to the failure of the slope. When averaged over the entire volume of the pit wall, the seismic velocity observations show a clear and sustained decrease following a mining blast that occurred on 11 February 2014. This decrease is unlikely to be explained by the effect of co-seismic shaking damage alone, and initiates nearly 14 days prior to the onset of the significant surface ground displacements and seismicity that marked the beginning of slope

failure. We believe that the signal detected in the temporal seismic velocity variations may indicate that the ultimate failure of the slope is related to the mining blast that took place at the foot of the pit wall, and could have provided earlier warning than the surface ground displacement and microseismic data.

We have also presented results from a novel process that allows us to map the distribution of temporal seismic velocity variations within a three-dimensional rock volume. Our results show that pre-existing geological structures are likely to place a critical control upon the response of a rock mass to a failure. In the case of Century Mine, we detect strong reductions in seismic velocity in a breccia wedge subsequent to the slope failure, which we interpret to be the result of increased fracturing in the rock unit as the slope fails. By contrast, the buttress located at the base of the unit exhibits a clear increase in seismic velocity, which may represent the closure of fractures following an increase in compressive stress caused by the slope failure. Two fault systems at Century Mine, the Page Creek Fault and the Pandora Fault, appear to separate two broad domains in the seismic velocity response to instability. In the region between the two faults, the rock exhibits broad increases in seismic velocity, particularly at the top rim of the pit wall. Outside the zone bounded by the two faults, broad zones of decreasing seismic velocity are found. Although it is possible that these zones of decreased seismic velocity could represent regions of meteoric fluid infiltration enabled by the faults, the role of rainfall and subsequent pore fluids in the stability of the slope remains unclear, with no general relationship obvious between daily rainfall and the geophysical observations. Nevertheless, our study has proven the efficacy of using observations of variability in rock mass seismic velocity as a monitoring tool that may be able to forecast slope instability, in addition to providing insight into the dynamics of a slope failure.

Acknowledgement

The Institute of Mine Seismology is thankful for the support of MMG Century Mine for their support of this research project and for permission to publish the data. In particular, we would like to thank Erin Sweeney, Kyle Abbott and Claudio Coimbra for their efforts.

References

Bensen, GD, Ritzwoller, MH, Barmin, MP, Levshin, AL, Lin, F, Moschetti, MP,... Yang, Y 2007, 'Processing seismic ambient noise data to obtain reliable broad-band surface wave dispersion measurements', *Geophysical Journal International*, vol. 169, pp. 1239–1260, https://doi.org/10.1111/j.1365-246X.2007.03374.x

Brenguier, F, Campillo, M, Hadziioannou, C, Shapiro, NM, Nadeau, RM & Larose, E 2008, 'Postseismic relaxation along the San Andreas Fault at Parkfield from continuous seismological observations', *Science*, vol. 321, pp. 1478–1481, https://doi.org/10.1126/science.1160943

Clarke, D, Zaccarelli, L, Shapiro, NM & Brenguier, F 2011, 'Assessment of resolution and accuracy of the moving window cross spectral technique for monitoring crustal temporal variations using ambient seismic noise', *Geophysical Journal International*, vol. 186, pp. 867–882, https://doi.org/10.1111/j.1365-246X.2011.05074.x

Le Breton, M, Bontemps, N, Guillemot, A, Baillet, L & Larose, E 2021, 'Landslide monitoring using seismic ambient noise correlation: challenges and applications', *Earth-Science Reviews*, vol. 216, https://doi.org/10.1016/j.earscirev.2021.103518

Luo, X, Salvoni, P, Dight, P & Duan, J 2018, 'Microseismic events for slope stability analysis - a case study at an open pit mine', *Journal of the Southern African Institute of Mining and Metallurgy*, vol. 118, pp. 205–210, http://dx.doi.org/10.17159/2411-9717/2018/v118n3a2

Obermann, A, Planes, T, Larose, E, Sens-Schonfelder, C & Campillo, M 2013, 'Depth sensitivity of seismic coda waves to velocity perturbations in an elastic heterogeneous medium', *Geophysical Journal International*, vol. 194, pp. 372–382, https://doi.org/10.1093/gji/ggt043

Paaschens, J. C. J. 1997, 'Solution of the time-dependent Boltzmann equation', *Physical Review E*, vol.56, pp. 1135–1141, https://doi.org/10.1103/PhysRevE.56.1135

Pacheco, C & Snieder, R 2006, 'Time-lapse travel time change of multiply scattered acoustic waves', *Geophysical Journal International*, vol. 165, pp. 485–500, https://doi.org/10.1111/j.1365-246X.2006.02856.x

Salvoni, M & Dight, PM 2016, 'Rock damage assessment in a large unstable slope from microseismic monitoring - MMG Century mine (Queensland, Australia) case study', *Engineering Geology*, vol. 210, pp. 45–56, https://doi.org/10.1016/j.enggeo.2016.06.002

Snieder, R, Sens-Schonfelder, C & Wu, R 2017, 'The time dependence of rock healing as a universal relaxation process, a tutorial', *Geophysical Journal International*, vol. 208, pp. 1–9, https://doi.org/10.1093/gji/ggw377

Taylor, G & Hillers, G 2019, 'Estimating temporal changes in seismic velocity using a Markov chain Monte Carlo approach', *Geophysical Journal International*, vol. 220, pp. 1791–1803, https://doi.org/10.1093/gji/ggz535